



Shaking-Table Test on a Multi-Story Continuous Vibration-Control System Employing Pulley Amplification Mechanism

Ryo Majima ¹, Yasuo Yamasaki ², Taiki Saito ^{1*}

¹ Department of Architecture and Civil Engineering, Toyohashi University of Technology, Toyohashi 441-8580, Aichi, Japan.

² Technical Research Institute, Nishimatsu Construction Co., Ltd, Tokyo 105-6407, Japan.

Received 06 October 2024; Revised 13 November 2024; Accepted 02 December 2024; Published 01 January 2025

Abstract

This study proposes an innovative passive vibration-control system, named the Pulley Damper Multi-story System (PDMAS), which incorporates pulley tackles installed at multiple stories in the successive stories to amplify inter-story displacement. This configuration significantly enhances the energy absorption efficiency of the linked dampers at the middle of the cable by utilizing the cumulatively amplified story displacements via a continuously stretched cable across the entire structure. The proposed system shows notable potential for controlling responses induced by higher vibration modes by customizing the wire installation layout. The aim of this study is to introduce PDMAS and to investigate its seismic-mitigation effectiveness. As a primary investigation of this new system, comparative experimental studies were conducted through shaking-table tests on nine specimens featuring various cable layouts optimized for the first and second structural vibration modes, with or without dampers, under harmonic waves, white-noise waves, and simulated seismic waves. The experimental results demonstrate that the PDMAS effectively accommodates the cumulative amplified story displacement across the structure to match theoretical damper values. Furthermore, the specimens employing PDMAS with a wire layout optimized for the first structural mode reduced both acceleration and displacement by nearly half compared to specimens without PDMAS.

Keywords: Passive Damper; Displacement-Amplification System; Pulley Mechanism; Nonlinear Viscous Damper; Shaking-Table Test; Shear-Deformation Specimen.

1. Introduction

Various types of earthquake-protection technologies designed to control building damage during a seismic event and ensure that buildings remain functionally sustainable are currently available [1]. Among these technologies, passive vibration-control structures are the most widely adopted for dissipating seismic energy by utilizing damping elements made from metals, friction, or viscous substances [2]. The most common configuration for attaching these dampers is installing them between two successive stories using a diagonal or chevron brace. The dampers generate a control force based on the relative displacement or velocity between the two attachment points. In such cases, based on the inclination angle of the dampers, the effective damper deformation is limited to either less than or equal to the maximum inter-story drift [3, 4]. Therefore, when dampers are conventionally applied to high-rise buildings and stiff structures that typically experience very small inter-story drift during an earthquake, the efficiency of some seismic-energy dissipation devices is reduced, and they can be underused.

Based on these considerations and to improve the energy-dissipation effect, several devices employing displacement-amplification techniques, which are mostly based on the toggle or seesaw mechanisms, have been implemented in actual

* Corresponding author: saito.taiki.bv@tut.jp

 <http://dx.doi.org/10.28991/CEJ-2025-011-01-02>



© 2025 by the authors. Licensee C.E.J, Tehran, Iran. This article is an open access article distributed under the terms and conditions of the Creative Commons Attribution (CC-BY) license (<http://creativecommons.org/licenses/by/4.0/>).

buildings [5-7]. These mechanisms allow the dampers to deform larger than the structural drift and amplify the damper output force, which depends significantly on the geometry configuration. This amplification results in an increase in the effective energy dissipation of a single damper and a reduction in the required damper volume and quantity in buildings.

In addition to the research of displacement amplification systems, while typical passive dampers perform damping force depending on their deformation in the axial direction, efforts are currently active in developing dampers that provide damping force against rotational deformations or relative angles to control structural seismic response [8-11]. Alhasan et al. [8] proposed a new rotational viscoelastic damper and the cyclic test results showed higher damping performance compared to the conventional shear deformation type viscoelastic damper.

Another approach is to use tension-only elements generally classified as damped cable systems (DCSs). This system accumulates the inter-story drift of multiple successive floors and translates large relative displacements to effectively activate a greater damping force. Pekcan et al. [12] initially proposed an effective method to control the seismic response, in which prestressed tendons were directly interconnected between the bottom and middle stories of steel-moment-frame structures, transferring the load from the structures to dissipative devices. Experimental verification using shaking-table tests on a six-story 1:4 scale steel plane frame revealed a reduction in the overall seismic response of the structure.

In a subsequent study, Pekcan et al. [13] presented a preliminary concept in which post-tensioned tendons, which were allowed to slide, were diagonally designed from the structure top to bottom, and they theoretically evaluated the effect of the supplemental tendon system. In addition, Stefano & Terenzi [14, 15] experimentally examined the feasibility of a DCS that included a prestressed steel cable with sliding connections to deliver the cumulative displacement from the top of the structure to a linked fluid damper anchored on a building foundation implemented in an RC structure. Correspondingly, some researchers showed that connecting the structure and damping device with cables efficiently improved the energy-dissipation capacity of individual dampers with minimal installation space [16-20].

Choi and Kim firstly proposed the installation scheme of a viscoelastic damper using cable and pulley, such that a cable is continuously stretched across all stories or selectively based on the structural vibration modes and thus enhancing the energy dissipation of the single damper linked to the cable [16]. By allowing the dampers to align with the overall story displacement rather than inter-story drift, this configuration maximizes damping efficiency, particularly in fundamental vibration modes. To evaluate the response reduction effect of the proposed cable-damper system, Choi and Kim carried out nonlinear time history analyses using full-scale 6- and 15-story structures. The results demonstrated that the cable-damper system significantly reduces damper size while achieving similar or better performance compared to conventional methods, and continuous cable setup showed high effectiveness in lower vibration modes. Additionally, Hernández et al. experimentally tested the cable system where combined a continuous single-thread cable is arranged along the specimen height and a spring damper is fixed at the specimen base [19]. Based on the shaking table test on a simplified 5-degree steel structure confirmed under different test conditions, including reference structure with and without damper or wire, Hernández et al. concluded that the proposed system could provide high damping ratios for all the structural modes and mitigate displacement and accelerations as well as the empirical response spectrum. The test result also suggested that the friction force generated between the cable and pulley sheave enhances damping and contributes to the seismic response reduction. However, as some researchers have discussed [16, 19], according to the structural mode shape and the location of pulleys, the continuous tendon layout may be ineffective in activating the damper capacity under the higher vibration mode because the cumulative inter-story displacements in the lower and upper structures are reduced or cancelled. Furthermore, the studies by Choi and Kim, and Hernández et al., use only one thread between each pulley. Consequently, due to the inclination angle of the cable being similar to that of a diagonal brace system, the damper is insufficiently activated when the structural deformation is small.

On the other hand, Saito et al. initially proposed the idea to use the pulley tackle to increase the inter-story displacement and maximize the energy absorption effect of the connected damper [21]. The damper displacement is amplified based on the number of threaded cables and the inclination angle between the pulley tackles. In addition to this, Saito et al. established the theoretical model considering the elastic deformation of the cable and then successfully confirmed the amplification effect of the damper displacement and damping force by the dynamic loading test. Recently, Jung et al. and Rouhani et al. carried out dynamic cyclic and seismic loading tests using a hydraulic actuator under different loading protocols, such as the number of threaded cables and pretension force [22, 23]. The test results verified that the pulley tackle system is capable of providing a large displacement amplification factor compared to the toggle configuration or lever-arm configuration. However, it has been pointed out that the true displacement amplification factor is slightly smaller than the theoretical value due to the friction force generated at the pulley-cable contact surfaces and the elastic deformation of the cables.

In previous works, authors proposed a new concept for a passive vibration-control system called the pulley damper amplification system (PDAS), which uses pulley systems to amplify the damper displacement [21]. Additionally, authors presented an application example of a PDAS in which the system was installed in a coupling structure such that the cable connects the top of the rigid and flexible structures [24]. The results of the shaking-table test demonstrated that

the proposed system maximized the energy-dissipation capacity of the damper and effectively mitigated the seismic response compared to the uncontrolled specimen. However, the response in the middle story was relatively excited owing to the second vibration mode, whereas the first-mode deformation was well-controlled.

The main goal of this experimental research is to expand and develop the cable-damper system by incorporating the PDMS and to propose the pulley damper multi-story amplification system (PDMAS). The key difference from the original single-threaded cable-damper system is that the newly proposed PDMAS employs multiple pulley tackles in series to amplify inter-story displacement through reciprocating threaded cables and deliver the cumulative amplified displacement to the damper. The expected advantage of the proposed system is its ability to improve the energy-dissipation efficiency of the linked damper by utilizing the cumulative amplified story displacement and mitigating the responses of multiple vibration modes.

The objective of this paper is to verify the delivery of the cumulative amplified story displacement to the damper, understand the frequency and mode characteristics of different wire arrangements, and evaluate the seismic-response reduction effect. This paper consists of the following: Section 1 summarized the damper-cable system and pulley tackle displacement amplification mechanism. It is then that section 2 introduces the underlying concept of the PDMAS with detailed illustration. Section 3 presents the design of six degrees of shear-deformation specimens with natural rubber bearings (NRBs) and the experimental setup. Section 4 shows the shaking table test results on nine specimens with and without dampers under different cable layouts subjected to white-noise waves, sinusoidal waves, and simulated earthquake waves. The experimental results are analyzed, evaluating the seismic-response reduction effect as well as the displacement amplification factor. Section 5 concludes this study and discusses future work.

2. Concept of the Proposed System

2.1. Pulley Damper Amplification System

Figure 1 shows the configuration and working principle of the proposed PDAS, which efficiently improves the energy-dissipation capacity of the damper. A previous study by Saito et al. [21] and similar studies by Jung et al. [22] and Rouhani et al. [23] experimentally verified the effect of the displacement amplification of the damper using pulley systems through full-scale frame tests using a dynamic actuator under several loading protocols.

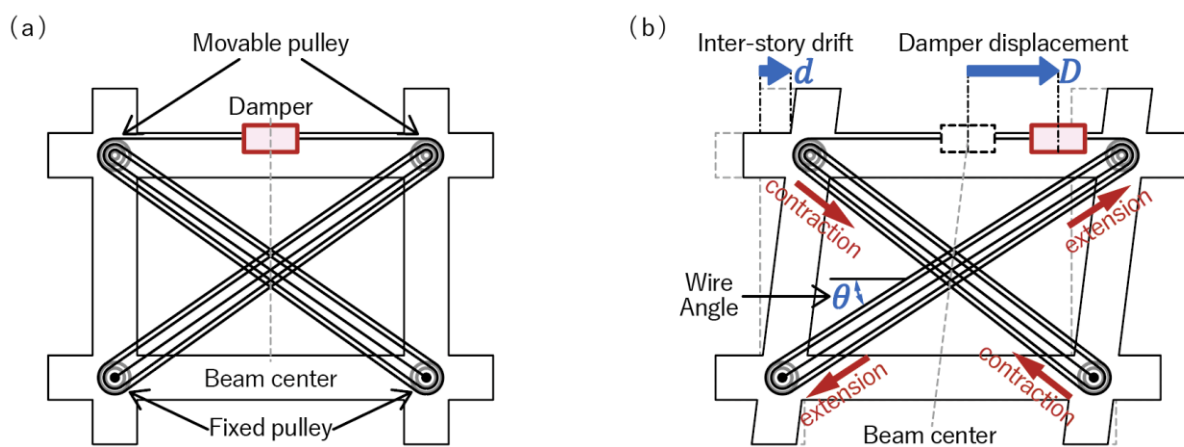


Figure 1. The operating mechanism of the PDAS: (a) stationary stage; (b) dynamic stage

As shown in Figure 1-a, the PDAS consists of a pulley, wire, and damper linked to the middle of the wire. The wire is symmetrically stretched between the fixed and movable pulleys multiple times at the center of the beam. When a lateral force induces shear deformation, one diagonal wire distance is extended while the opposite wire is contracted. Assuming the inter-story drift due to lateral force is d and the wire inclination is θ , the incremental displacement along the diagonal length is $d \times \cos \theta$. In the case where the wire threaded n times between the pulleys, the total diagonal displacement which is equal to the damping displacement can be expressed as Equation 1. Therefore, the displacement of the wire movement can be easily controlled, depending on the number of reciprocated wires between the stationary and movable pulleys.

$$D = d \times n \times \cos \theta \tag{1}$$

2.2. Pulley Damper Multi-Story Amplification System

Whereas most dampers are activated by a certain inter-story drift, the proposed PDMAS utilizes a large relative displacement, which accumulates inter-story drifts located below the damper. A conceptual diagram of the proposed wire-installation layout is shown in Figure 2. To demonstrate the working principle, two different types of wire layouts

are considered for installation in a two-story structure: a wire arrangement optimized for first-mode deformation and the other for second-mode deformation. In this configuration, six pulleys are fixed at the base, middle, and top stories, and the damper is installed only on the top story. The wires in each diagonal part have 2.5 loops.

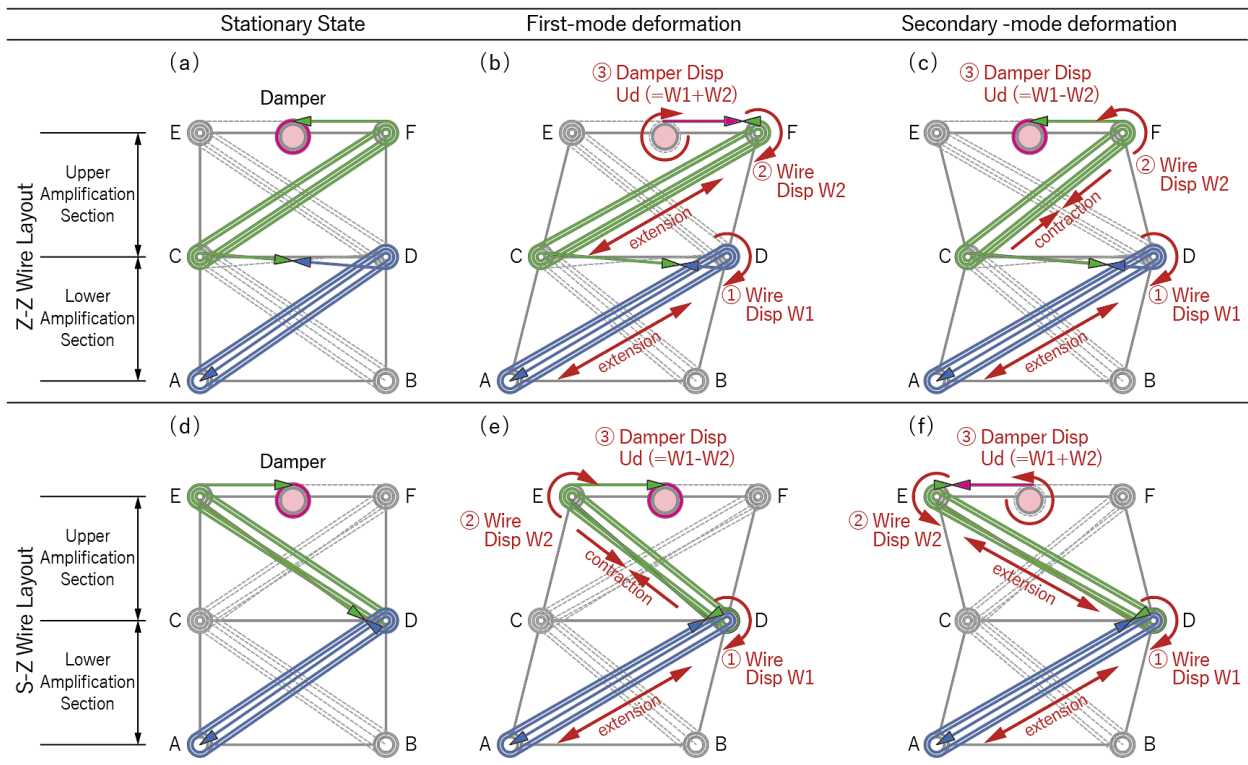


Figure 2. Installation scheme of the proposed system

Compared to the conventional PDAS, which includes only a single story with a reciprocating wire segment (see Figure 1), as illustrated in Figure 2, the PDMAS applies the unit of reciprocating wire segment across multiple successive stories. Therefore, assuming frictionless pulley tackles and no slack in the cable, the ideal cumulative damper deformation, D_{cum} can be expressed as:

$$D_{cum} = \sum_{i=1}^k d_i \times n_i \times \cos \theta_i \tag{2}$$

where k is the total number of stories with reciprocating wire segments, and d, n, θ represent the inter-story drift, the number of threaded cables, and the wire inclination angle at story i , respectively.

Figure 2-a illustrates a continuous wire layout stretching throughout the structure’s bottom to middle stories (A-D) and middle to top stories (C-F) in parallel (hereinafter, this type of wire layout is named “Z-Z”). Conversely, in Figure 2-d, the continuous wire from the bottom to middle stories (A-D) and middle to top stories (D-E) is designed to be intersected at the middle story (hereinafter, called “S-Z”). As shown in Figure 2-b, when the structure with the Z-Z wire layout is deformed horizontally by its first vibration mode, the wires in both the lower and upper sections turn into extension members, thereby successfully transferring the cumulative displacement to the damper. Assuming the relative wire displacements at lower and upper stories are $W1$ and $W2$, the ideal damper displacement D_{cum} would be $W1 + W2$. However, as shown in Figure 2-c, if the structure is moved by its second-mode deformation, the lower section maintains extension deformation, whereas the upper section changes to a contraction member. Because the wires in the lower and upper stories are continuous, the summation of the total wire movement may be mutually cancelled, and the damper does not dissipate energy.

To address this problem, another wire layout is necessary to activate the damper under second-mode deformation. Figure 2-b illustrates the S-Z wire layout optimized to maximize the displacement of the damper when the structure deforms in the second mode. In this case, similar to Figure 2-c, if it is shaken by the first vibration mode, the lower and upper members show different deformations in opposite directions; therefore, the total wire displacement at the damper location is zero, and the damper cannot deform. However, as expected, this layout shows a good response with the second vibration mode and enables the use of the cumulative displacement to activate the damper.

3. Experimental Program

3.1. Six-Story Shear-Deformation Specimen

To verify the performance of the effective operation of the proposed system and investigate the frequency characteristics, comparative shaking-table tests were conducted on a triaxial shaking table with six controlled degrees of freedom at the Structural Engineering Laboratory at Nishimatsu Construction Co., Ltd., Japan, in January and February 2024. The shaking table has a payload capacity of 30 tons and dimensions of 5.5×5.5 m. Figure 3 shows the details of the test structure. The specimen was fabricated to have only shear deformation in one direction and maintain linear elastic behavior even under repeated excitations. Similar experimental studies that modeled the target structure using concrete slabs or steel plates for lumped masses and coil springs or seismic isolators for their equivalent stiffness can be found in [25-28].

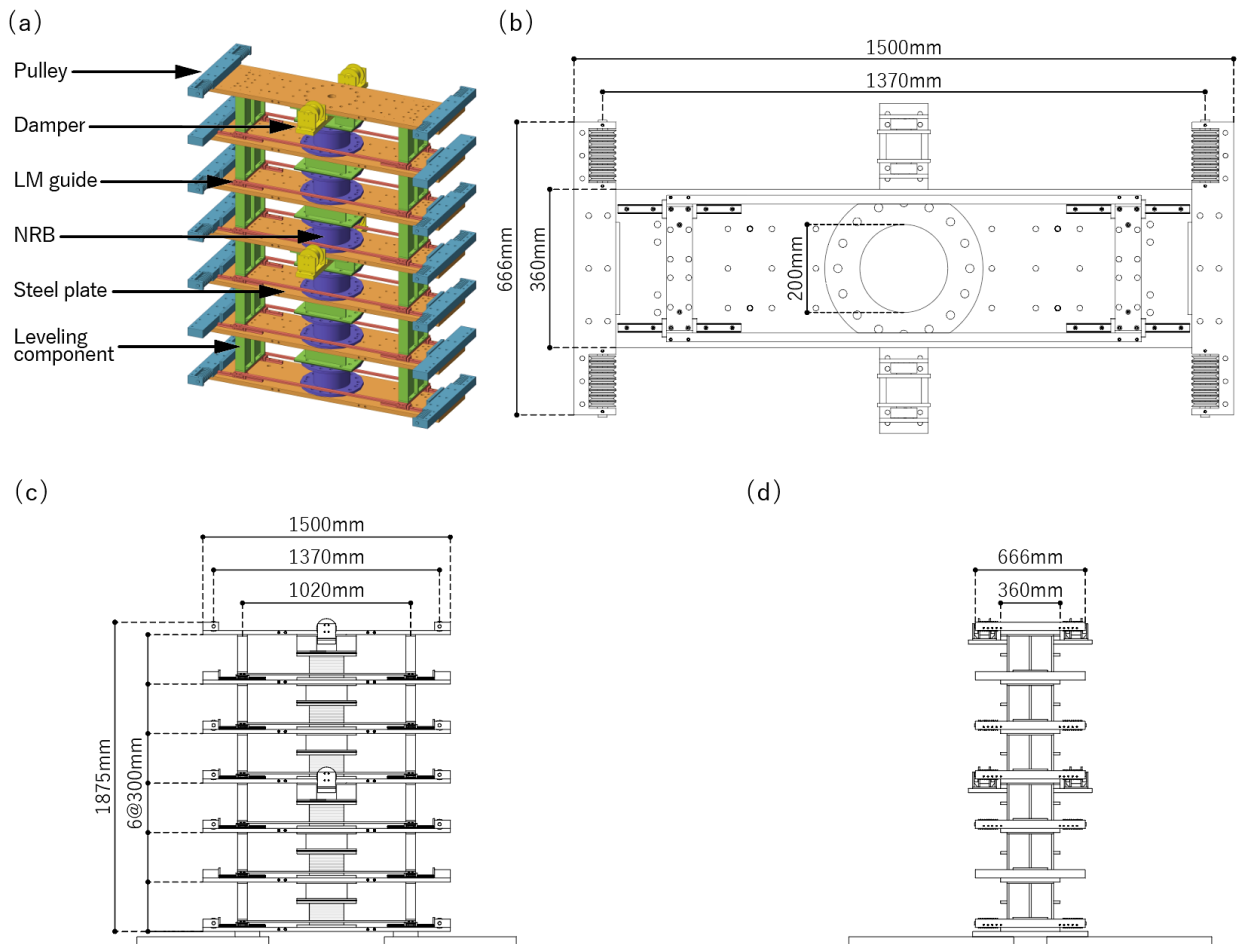


Figure 3. Six-story shear-deformation specimen: (a) perspective view; (b) plan view; (c) front view; (d) right side view

The first fundamental frequency of the specimen was approximately 1 Hz. The overall size of the specimen was 1500 mm × 300 mm × 1875 mm, and the total mass was 1.6 tons. As shown in Figures 3-a and 3-b, every story consisted of a main steel plate, an NRB with a diameter of 200 mm and height of 132 mm placed on the floor center, four linear motion (LM) guides, two pulleys, and several leveling components on the LM guides and NRB. The floor size was 1500 mm × 300 mm, with a thickness of 25 mm, and the inter-story height was 300 mm. The story stiffness and restoring force were provided by the NRBs placed at the center of the floor, and the fundamental period was controlled by the mass of the floor plate. The horizontal stiffness of the NRBs is 117 N/mm, based on the manufacturer's unidirectional sinusoidal-wave element tests under 75 kN vertical load with 105% shear strain. The story mass is about 245 kg.

Additionally, the LM guides were installed at each floor corner to restrain the bending deformation of the specimen during excitation. The diameter of the pulley sheave was 50 mm, with a single-row ball bearing inside, and each pulley had nine independent sheaves.

3.2. Specimen List

Nine test specimens were selected based on the presence or absence of dampers and wire layout. The parameters and detailed conditions included in these nine test series are summarized in Figure 4 and Table 1. The abbreviation in the

first half of the specimen’s name indicates the presence of the frame (F), wires (W), and dampers (D), while the second half indicates the wire layout (the symbols “+” and “-” denote a discontinuous and continuous wire, respectively).

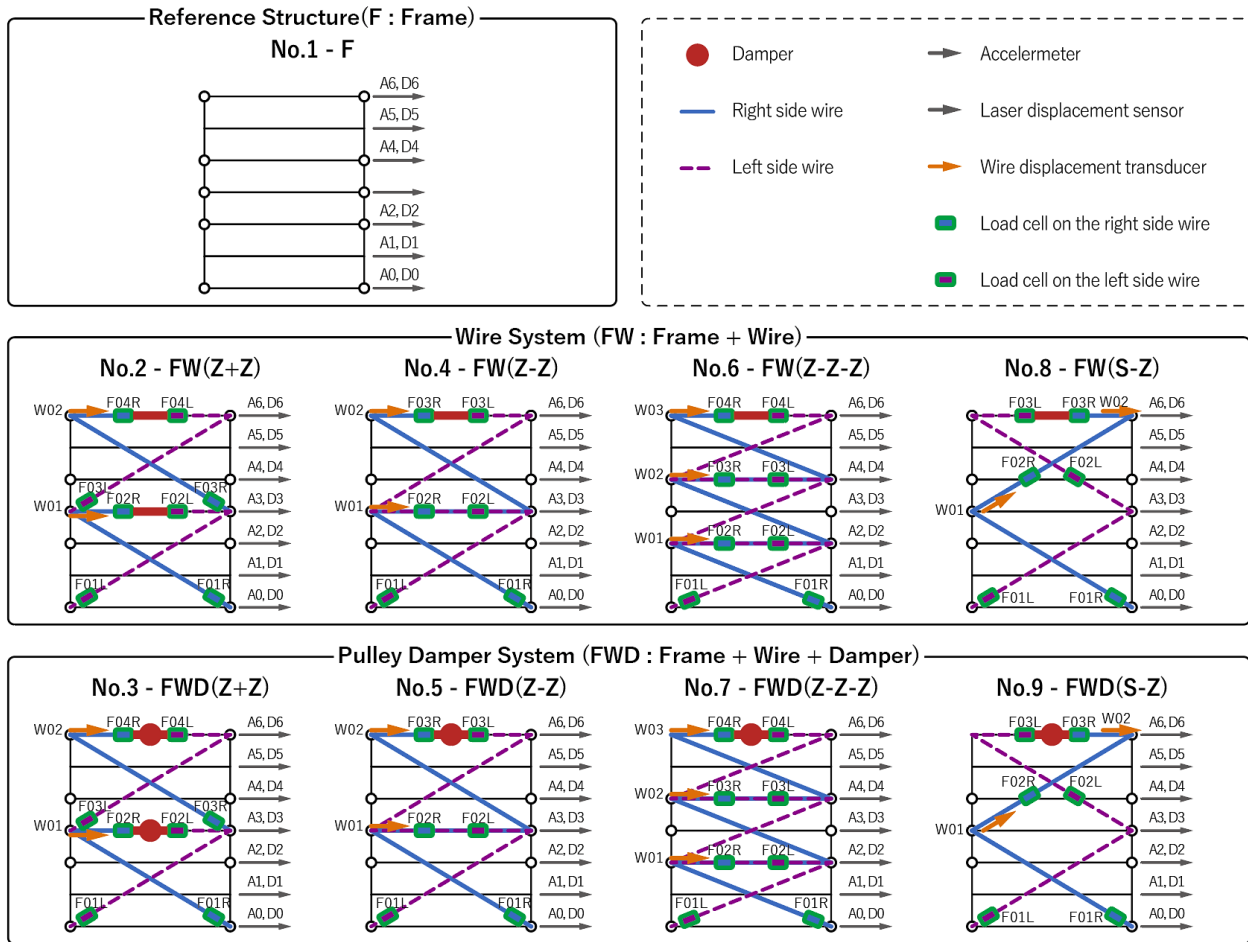


Figure 4. Test configurations and measurement-equipment location of each specimen

Table 1. Details of specimen condition

| Specimen number | Specimen name | Number of diagonally reciprocated wires | Rotational damper | Amplification factor | Theoretical wire length |
|-----------------|---------------|---|-------------------------|-----------------------------------|---------------------------|
| No.1 | F | No | No | No | No |
| No.2 | FW(Z+Z) | 5 | No | $4.2 = 5 \times \cos(33.3^\circ)$ | $19.2 \text{ m} \times 2$ |
| No.3 | FWD(Z+Z) | 5 | Third and sixth stories | $4.2 = 5 \times \cos(33.3^\circ)$ | $19.2 \text{ m} \times 2$ |
| No.4 | FW(Z-Z) | 5 | No | $4.2 = 5 \times \cos(33.3^\circ)$ | 38.4 m |
| No.5 | FWD(Z-Z) | 5 | Sixth story | $4.2 = 5 \times \cos(33.3^\circ)$ | 38.4 m |
| No.6 | FW(S-Z) | 5 | No | $4.2 = 5 \times \cos(33.3^\circ)$ | 38.4 m |
| No.7 | FWD(S-Z) | 5 | Sixth story | $4.2 = 5 \times \cos(33.3^\circ)$ | 38.4 m |
| No.8 | FW(Z-Z-Z) | 3 | No | $2.7 = 3 \times \cos(23.7^\circ)$ | 35.2 m |
| No.9 | FWD(Z-Z-Z) | 3 | Sixth story | $2.7 = 3 \times \cos(23.7^\circ)$ | 35.2 m |

Specimen No.1, a reference structure without a wire and damper installation, was firstly tested to examine the dynamic behavior of the fabricated six-story shear-deformation specimen. Specimens No.2 and No.3 had two pulley damper systems, where the wire was disconnected in the lower (between the base and third stories) and upper (between the third and sixth stories) stories, to compare the seismic-reduction effect of the proposed system. Specimens No.4 and No.5 had a continuous wire with a Z-Z layout optimized for the first-mode deformation, and specimens No.6 and No.7 had an S-Z wire layout developed for the second-mode deformation. Finally, specimens No.8 and No.9, which stretched the diagonal wire in the lower (between the base and second stories), middle (between the second and fourth stories), and upper (between the fourth and sixth stories) stories, were investigated.

To prevent torsional behavior of the specimen during the tests, a wire and damper with the same layout were installed on the front and back sides of the test specimen. The wire installation angles listed in Table 1 were calculated based on the center distance of the pulley shaft.

3.3. Test Setup and Measurement Equipment

Figure 5 shows the experimental setup of FWD (Z-Z) and enlarged photographs of the specimen components. As shown in Figure 5-a, the test specimen was mounted at the center of the shaking table, and a rigid frame with a natural frequency of 18 Hz was placed around it to install the measurement equipment. Figure 5-b shows the main damping device, which is explained in detail in Section 4.3, (c) shows a pulley on the third story where the wires on the left and right sides intersect, and (d) shows the anchorage and pretension method of the wire.

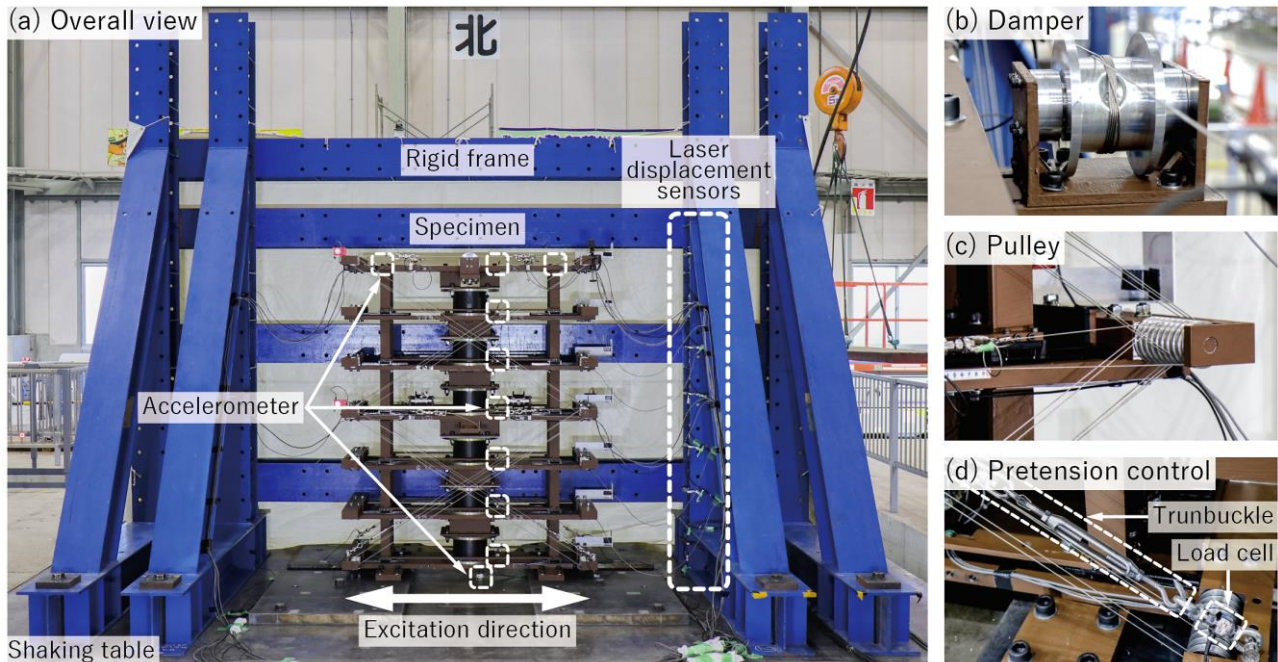


Figure 5. Test setup of FWD(Z-Z)

Figure 4 shows the locations of the measurement equipment on the specimens. During the experiments, data were acquired at a sampling rate of 500 Hz. The absolute acceleration in the excitation direction of each floor on the test specimen and the three directions at the top of the specimen and shaking table surface were measured using strain gauge-type accelerometers (ARF-20A; Kyowa Electronic Instruments Co., Japan). The relative displacement of each story with respect to the shaking-table surface was recorded using laser-displacement sensors (LK-500, Keyence Co., Japan) arranged on the rigid frame.

The tensile force and movement of the wire were directly measured using load cells (LUR-A-500NSA1; Kyowa Electronic Instruments Co., Japan) and a wire displacement transducer (DP-1000G; Tokyo Measuring Instruments Laboratory Co., Ltd., Japan) equipped before and after the wire was threaded diagonally. The wire displacement transducers were firmly fixed to the floor plate and recorded the absolute wire displacement. For the wire cable, a stainless-steel strand wire with a 1.5 mm diameter and 7×19 profile configuration was used, which is known to have a high degree of flexibility and strength. The breaking force of the wire was 1.95 kN, Young's Modulus is about 120 kN/mm², and 40% of the wire-rope breaking strength (0.78 kN) was applied as pre-stressed tension to remove the influence of the initial stretch and ensure the wire steels into a stable condition during the experiment.

3.4. Excitation Program

Shaking-table tests were performed using three motions: white-noise waves, sinusoidal waves, and simulated earthquake waves (Figure 6).

White-noise-wave tests were performed for each configuration to identify the natural vibration frequencies and corresponding mode shapes. The white-noise-wave band at 0.1–50 Hz was generated with a flat power spectral density of 100 cm/s². The amplitude of the white-noise wave gradually increased until it reached the predominant frequency of the Fourier-spectrum ratios between the base and top story. Subsequently, the preliminary and secondary vibration frequencies were determined, and harmonic excitation tests using sinusoidal waves were conducted to confirm the behavior of the specimen and damper system at the corresponding resonant frequencies.

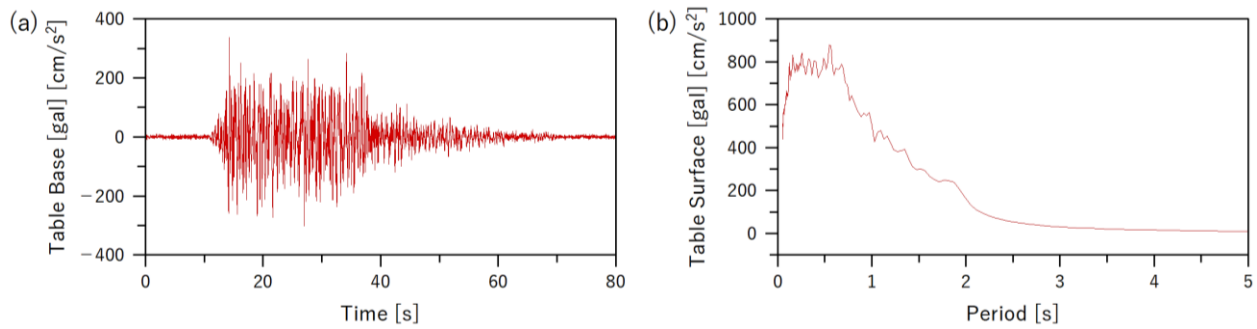


Figure 6. Inputted simulated earthquake wave: (a) acceleration time history; (b) acceleration spectrum.

The dynamic properties of the test specimen were examined using a simulated earthquake motion, hereafter the Art-wave, designed to match the seismic demand specified in the Japanese Building Code. This simulated wave, widely used in engineering practice in Japan, was generated with a random phase to ensure that the shaking table test provides a realistic representation of the structural response under expected seismic conditions. The wave had a peak spectral acceleration of approximately 800 cm/s², corresponding to a Level II earthquake at the bedrock, with a peak ground acceleration (PGA) of 340 cm/s² and a duration of 60 seconds. The acceleration wave and acceleration response spectrum of a 5% damping ratio are shown in Figure 6. The available range of the wire movement was limited to approximately 300 mm owing to the positioning of the load cell on both sides of the damper. Therefore, the input level was gradually increased to ensure that the load cell did not contact the test specimen.

During the shaking-table test, an initial pre-tension force was introduced and controlled to the wire by tightening the turnbuckle anchored at the base of the specimen (see Figure 5-d) to eliminate wire slackness when the direction of the wire movement changed from forward to backward [29, 30]. In this test, the pre-tension force for the wire was set to 120 N, which was 1.5 times larger than the maximum estimated damper force, and was adjusted before every excitation by monitoring the measurement values from all installed load cells.

4. Dynamic Properties of the Specimen Elements

4.1. Frequency Characteristics of the Reference System

The frequency characteristics of the reference structure, specimen No.1 without the wire and damper installation, were initially identified based on the Fourier-amplitude ratio between the base and top stories of the specimen. In this study, during the computation of the Fourier spectrum for the frequency-domain characteristic-analysis, the Hannig-windowing technique was applied with a 75% overlap over 4096 points along the time axis of the absolute-acceleration time histories.

Figure 7 summarizes the transition of the primary natural frequency in the left vertical axis and inter-story drift of each story in the right vertical axis under white-noise excitation. The primary frequency was initially 3.17 Hz under 10% white-noise excitation when all inter-story displacement was less than 0.1 mm (1/3000 rad), due to the influence of the initial stiffness of the friction force at the LM guides generated between the LM block and its rail. It is then that the peak frequency ratio converged to 1.10 Hz after the inter-story drift exceeded 0.5 mm (1/300 rad) at 200% excitation. This result indicates that the actual natural frequency of the reference structure is estimated to be 1.10 Hz.

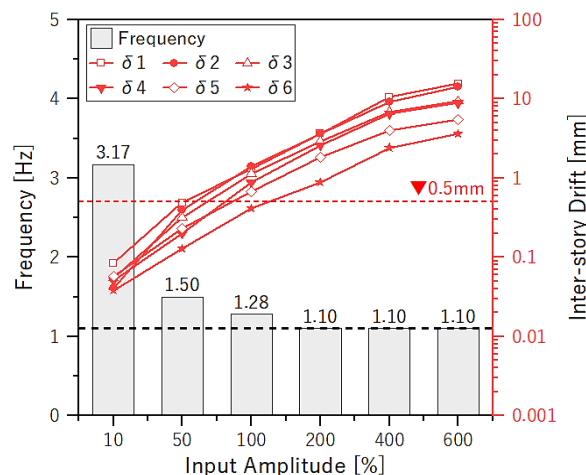


Figure 7. Primary natural frequency and the inter-story drift relation of the uncontrolled specimen

The damping coefficient of the reference structure was determined based on a free-vibration test. A forced displacement amplitude of approximately 100 mm was obtained by directly pulling the top story using a chain block. The displacement response of the top story is shown in Figure 8. According to the logarithmic decrement method, the damping ratio of the entire system was defined to be 7.3%. Notably, this high damping coefficient was affected by the existence of the NRBs and LM guides on each story.

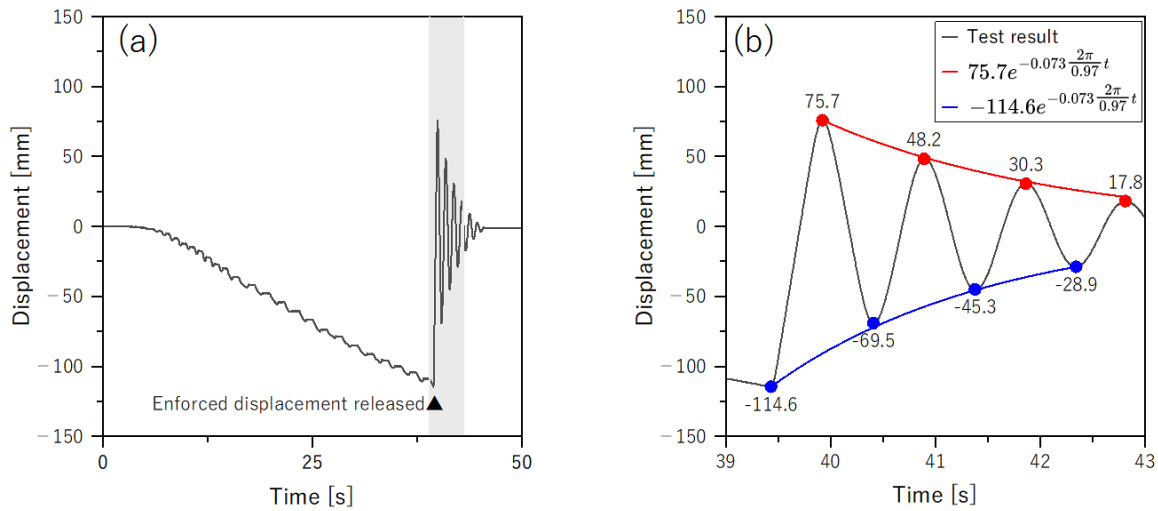


Figure 8. Free-vibration test result of the top story: (a) displacement time history; (b) test result with logarithmic decrement curve

4.2. Rotational Damper Properties

A newly designed and fabricated rotational damper, capable of accommodating a large wire displacement by pre-winding the wire several times around the spool, is depicted in Figure 9. The rotary damper (TOK, Inc., Japan, TD58-8K) shown in Figure 9-b, which can operate at infinite angles and produce a damping force by utilizing the fluid resistance of the silicone oil as the damper rotates, was selected as the main energy-dissipation element. Additionally, the rotational damper included ball bearings and other supports for stable operation, ensuring the smooth transfer of the horizontal wire movement to the damper without the shaft swing. The main feature of this damper was that, theoretically, the displacement range could be made unlimited by increasing the amount of wire wound around the spool. In addition, because the rotary damper provided nonlinearity in the velocity-force relationship, the maximum damping force could be limited.

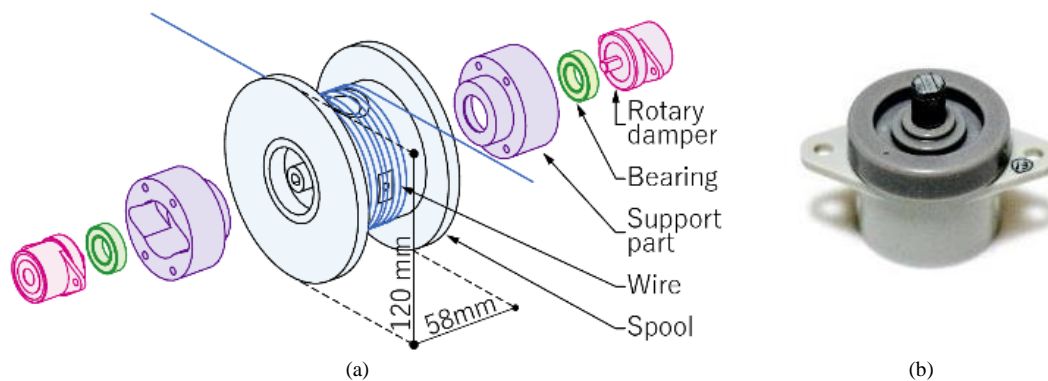


Figure 9. Details of rotational nonlinear viscous damper: (a) the assembly sequence of the damper; (b) a photograph of the rotary damper used in the test

Prior to the shaking-table experiments, the proposed damper was tested under displacement-controlled sinusoidal waves at various frequencies to investigate its damping characteristics. The test setup is illustrated in Figure 10. A small shaking table, with a payload capacity of 1000 N, and a maximum horizontal amplitude of 40 mm were utilized as the dynamic actuators, and the pulley mechanism (P1 and P2 in Figure 10) was employed to magnify the wire displacement from 40 to 300 mm. A pretension force of 120 N was given by the counterweight, and the damping force was calculated from the tensile-force difference between the two load cells (F1 and F2 in Figure 10) inserted on both sides of the damper. The displacement of the damper was indirectly measured by the movement of the load cell using a wire-displacement transducer.

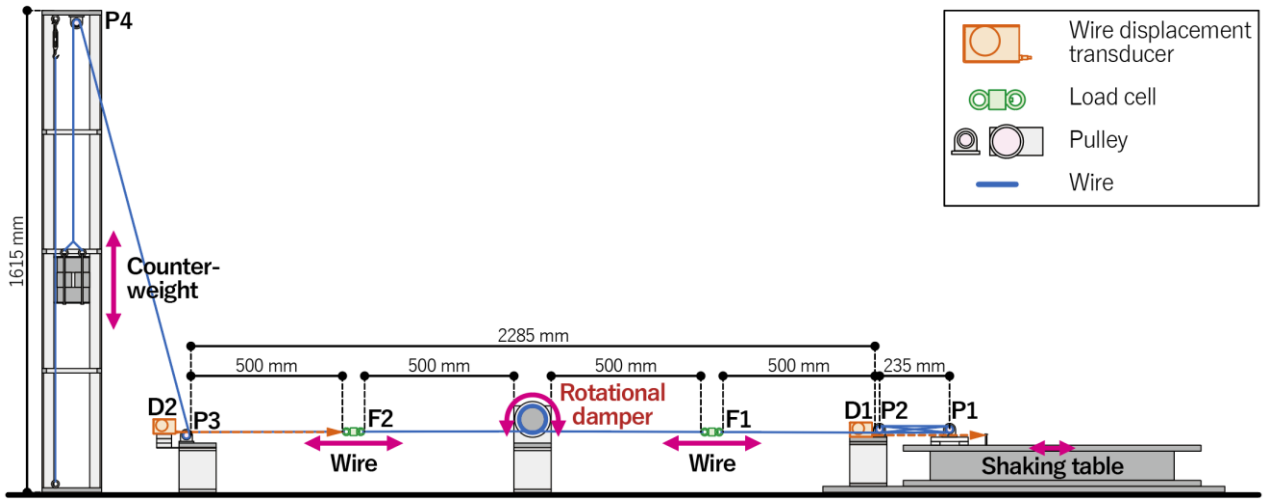


Figure 10. Test setup for the element test of the rotational damper

The test results at the frequency range between 0.1 Hz and 0.5 Hz are presented in Figure 11. The velocity-force hysteresis curve shows the nonlinear characteristics of the damping force. Therefore, the force-displacement relationship is given by Equation 2 using a simplified Maxwell model, in which the damping force is proportional to the exponent of the velocity:

$$F_v = C_d \times \text{sgn}[\dot{x}(t)]|\dot{x}(t)|^\alpha \tag{3}$$

where, sgn is the signum function, $\dot{x}(t)$ is the relative velocity of the wire, C_d is the damping constant, and α is the exponential constant.

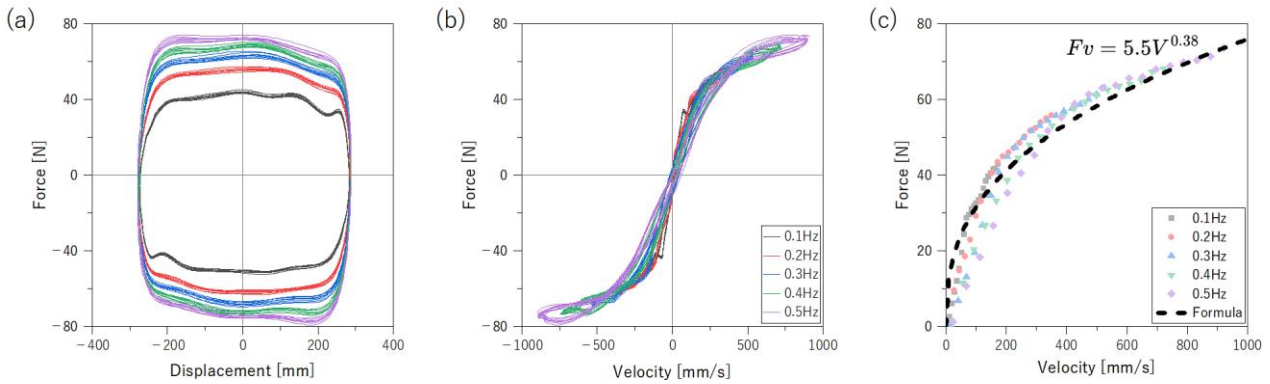


Figure 11. Test results of the element test of the rotational damper: (a) damper displacement-force hysteresis; (b) damper velocity-force hysteresis; (c) damper velocity-force relationship

Figure 11-c shows the average damping force at each velocity segment and the approximate formula for the damper. The damping coefficient and exponent value are set to be in good agreement with the experimental results, and C_d and α are defined as $5.5 \text{ N}\cdot(\text{s}/\text{mm})^{0.38}$ and 0.38, respectively.

4.3. Friction of Pulley

The frictional resistance at the contact between the pulley and wire, including the bearings inside the pulley sheaves, affected the dynamic properties of the proposed system. The friction force was investigated based on a sinusoidal dynamic test at various pre-tension forces (80, 100, and 120 N) and the numbers of wire loops (1, 3, and 5 loops). Figure 12 shows the setup for the friction-element test. The F1 load cell was fixed at the start of the blue wire, and another F2 load cell was installed at the end of the wire. The friction force was indirectly calculated from the difference of two tension forces obtained at load cells F1 and F2. Similar to the rotary damper test, a shaking table was utilized as a dynamic actuator, and the pre-tension force was controlled by changing the number of counterweights.

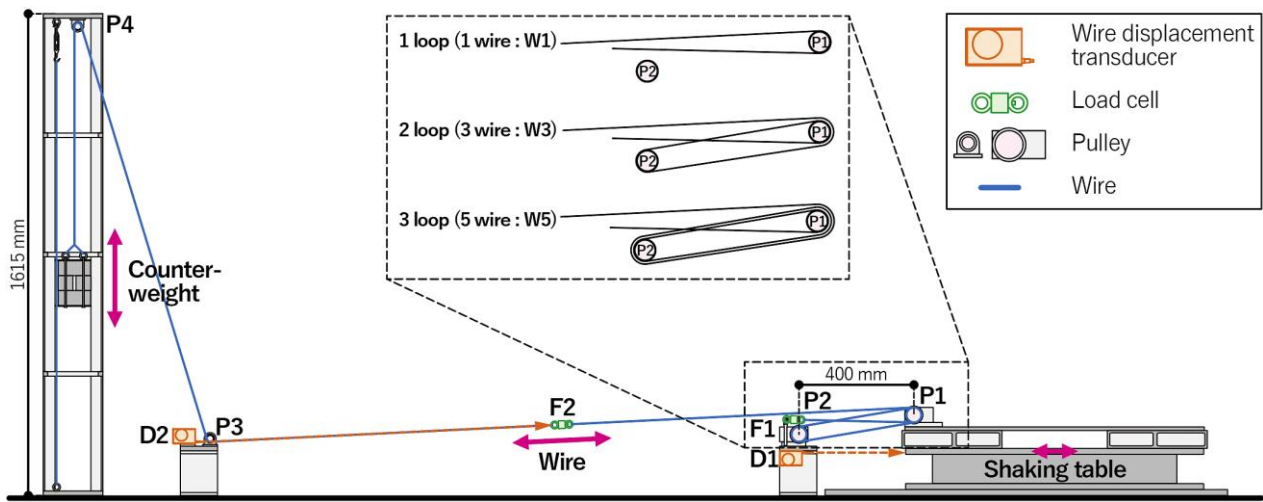


Figure 12. Test setup for the element test of the friction on the pulleys

Figures 13-a and 13-c show ten cycles of the displacement-force relationship for each test. The hysteresis loops show a rectangular shape, which is a characteristic of friction behavior. Additionally, as shown in Figure 13-d, the average friction force increased as the number of loops and pre-tension force increased. To normalize the relationship between the friction force and the product of the pretension force and number of wire loops, denoted as μ for the coefficient of friction, the following equation can be established:

$$F_y = \mu \times (n \times P_{initial}) \tag{4}$$

where F_y denotes the frictional force, n is the number of wires between the fixed and movable pulleys, and $P_{initial}$ is the pretension force.

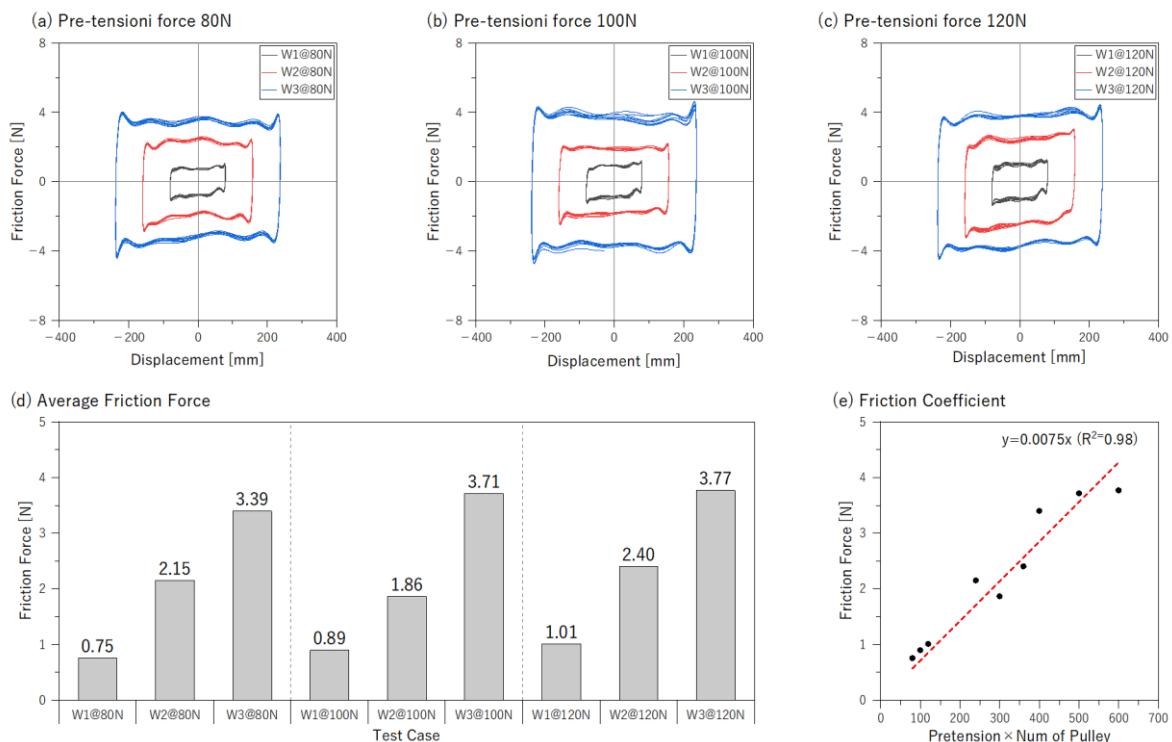


Figure 13. Friction test results: (a-c) friction displacement–force hysteresis for each pretension force; (d) friction force; (e) friction coefficient

Figure 13-e presents the friction force on the vertical axis and the product of the number of wires and pretension force on the horizontal axis. A linear correlation was observed between the two axes. Based on Equation 3, the gradient corresponding to the friction coefficient was defined as 0.0075. During the test, a pre-tension force of 120 N was introduced to the wire; therefore, the friction force at each pulley sheath was estimated to be approximately 1 N.

5. Experimental Test Results for the Six-story Shear Deformation

5.1. Frequency and Vibration Mode Shape

The natural frequencies of the first two or three identified modes and the corresponding vibration-mode shapes are shown in Figure 14. The natural frequencies of the uncontrolled specimen are 1.10, 3.54, and 5.62 Hz for the first, second, and third modes, respectively.

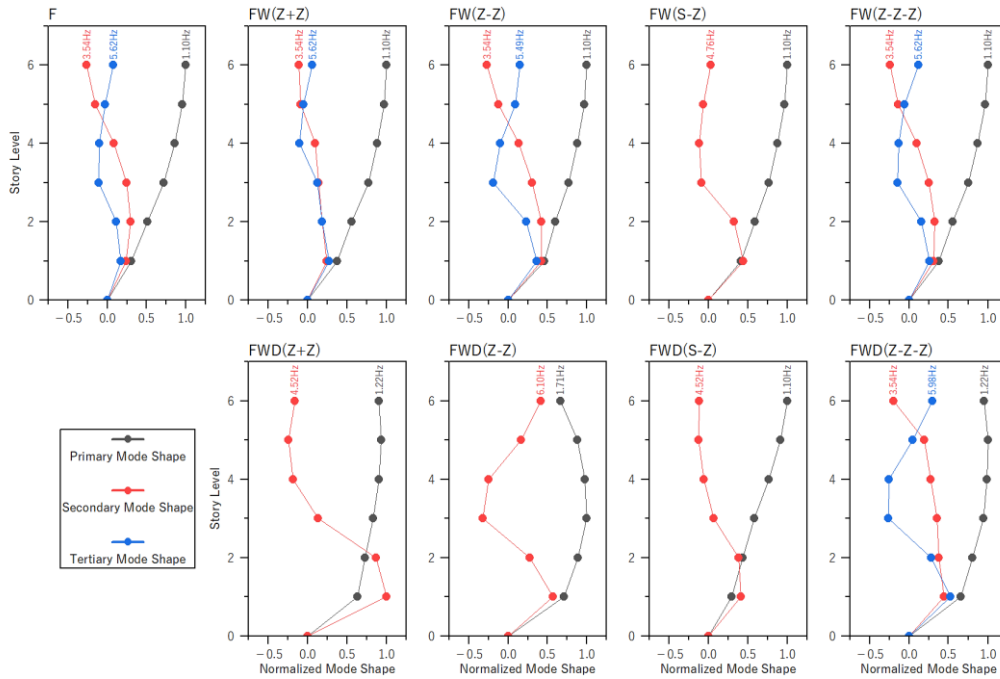


Figure 14. Normalized vibration-mode shapes

When comparing the natural frequencies and mode shapes of the uncontrolled specimen (F) and wire-system specimen (FW), no significant differences were observed. However, the secondary mode shape of FW(S-Z) exhibited frequency characteristics similar to the tertiary mode shapes of the other specimens. This occurred because FW(S-Z) had an optimized wire arrangement for second-mode deformation, effectively suppressing the second-mode vibration response and shifting the third-mode shape to the position of the second-mode shape. Similarly, comparing the mode shapes of the uncontrolled specimen (F) and the proposed damper system (FWD), the secondary-vibration mode shape of the FWD specimen exhibited a mode shape comparable to that of the third-vibration characteristic of specimen F because the second-vibration mode was well controlled by the installed damper.

5.2. Wire Displacement Under Sinusoidal-Wave Excitations

To confirm the effect of the cumulative-wire movement of the proposed system, Figure 15 shows the time history data of absolute wire displacement under sinusoidal-wave excitation for the wire-system specimen with a continuous wire from the specimen bottom to the top.

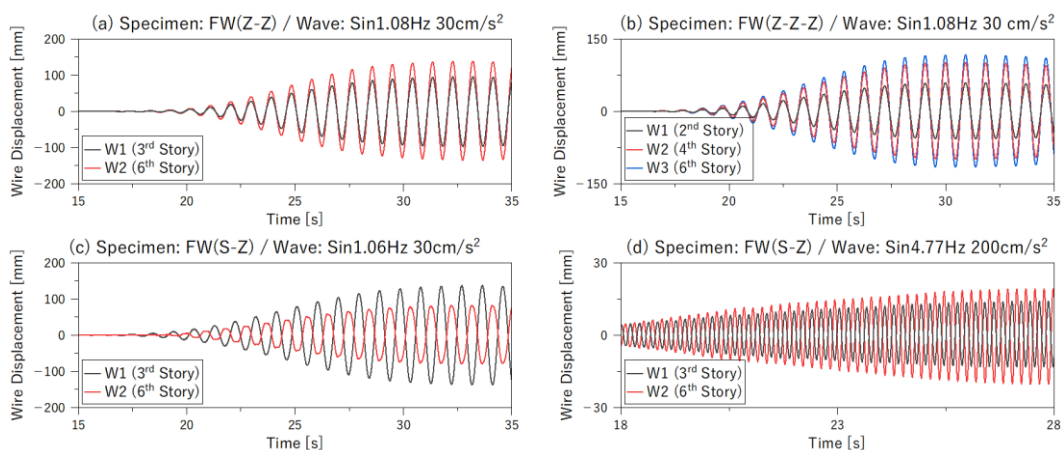


Figure 15. Time history of wire displacement under sinusoidal-wave excitations

As shown in Figures 15-a and 15-b, when FW(Z-Z) and FW(Z-Z-Z), which had wire layouts optimized for the first-mode shape, were excited by a sinusoidal wave corresponding to their first natural frequency, the wire displacements at the sixth story exhibited the largest response because the cumulative wire displacements of the lower story were successfully delivered to the top story. When the test specimen vibrates in the first mode, the inter-story displacement decreases with each higher story. Thus, in all results, the cumulative displacement in the wires gradually decreases as the story level increases. However, in the case of the FW(S-Z) specimen optimized for the second-mode vibration, which experienced sinusoidal vibrations at the primary frequency, the wire displacements at the sixth story were smaller than those at the third story, as shown in Figure 15-c. This is because the amplified displacements at the lower and upper sections of the structure cancelled each other out, as discussed in Section 2.2. Conversely, as shown in Figure 15-d, when FW(S-Z) was subjected to sinusoidal vibrations at the secondary frequency, a larger displacement was observed at the top story. Here, the phases of the wire displacements of FW(S-Z) at the third and sixth stories were in the reverse direction, as the deformation directions at the third and sixth stories under the second-mode shape were opposite.

5.3. Seismic Response

Figure 16 shows the maximum seismic response of acceleration, displacement, inter-story drift, and shear force under Art-wave 40 % excitation (PGA 145 cm/s²). The solid black line is the result of the uncontrolled specimen F, the dashed colored line represents the wire-system specimen FW, and the solid-colored line represents the damper system specimen FWD. Furthermore, the acceleration and displacement response-reduction effects of the proposed system on the sixth story are visually compared in Figure 17. Here, the response-reduction factors of the wire system β_{FW} and damper system β_{FWD} are defined as follows:

$$\beta_{FW} = \frac{\alpha_{FW,max} - \alpha_{F,max}}{\alpha_{F,max}} \times 100 [\%] ; \beta_{FWD} = \frac{\alpha_{FWD,max} - \alpha_{FW,max}}{\alpha_{FW,max}} \times 100 [\%] \tag{5}$$

where $\alpha_{F,max}$, $\alpha_{FW,max}$, and $\alpha_{FWD,max}$ are the maximum responses of the uncontrolled wire and damper systems, respectively.

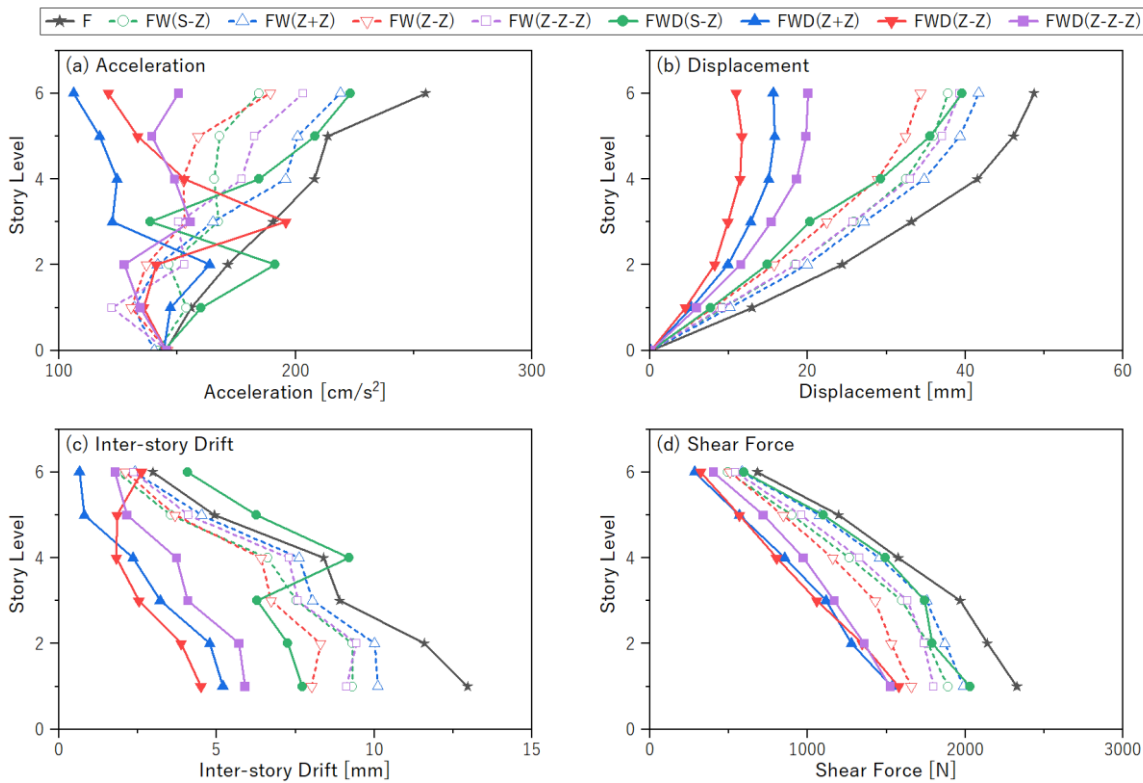


Figure 16. Comparison of the maximum structure response

Comparing the results of specimens F and FW, seismic responses at all stories showed smaller values for specimen FW than for the uncontrolled specimen F. For example, as shown in Figure 17, the top acceleration and displacement responses were reduced by an average of 22%. This response reduction was attributed to the energy-absorption effect of the friction force at the wire and pulley contacts, as discussed in Section 4.3.

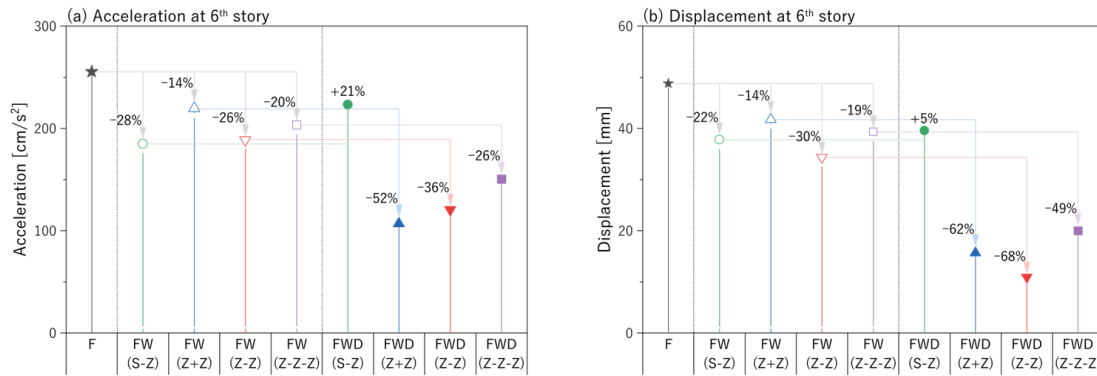


Figure 17. Comparison of the maximum response-reduction ratio

Additionally, specimen FWD included the proposed damper system, mitigating the entire story displacement, inter-story drift, and shear force, as well as the upper story acceleration response, compared with both specimens F and FW. This is because of the effect of the installed rotational damper. The response-reduction ratio of the proposed system can be clearly observed by comparing the maximum responses of specimens FW and FWD. The proposed system successfully reduced the displacement response by more than 50% compared with the specimen with only a wire. However, only FWD(S-Z), optimized for the second vibration-mode shape, was unable to reduce the seismic response, likely because the selected Art-wave was not strong enough to excite the second vibration-mode shape, and the first-mode deformation was dominant. For FWD(S-Z), the maximum damper displacement was only 15 mm, while it reached 43.6 mm for FWD(Z-Z). This difference in damper displacement resulted in a lower vibration mitigation effect for FWD(S-Z).

In the comparison of specimen FWD, the continuous wire specimen FWD(Z-Z) minimized the displacement response, and the discontinuous wire specimen FWD(Z+Z) exhibited the smallest acceleration. The overall responses of the FWD(Z-Z-Z) were slightly bigger than the FWD(Z+Z) and FWD(Z-Z) because FWD(Z-Z-Z) has a lower displacement amplification factor than other cases as shown in Table 1. However, since FWD(Z-Z-Z) connects three stories, the concentrated acceleration response seen at the second story of FWD(Z+Z) or the third story of FWD(Z-Z) was not observed. No differences in the shear-force results were observed, but a significant difference in the response characteristics of each story was observed in the acceleration response. While FWD(Z+Z) and FWD(Z-Z-Z) effectively reduced the acceleration response of the entire story, the acceleration response of FWD(Z-Z) at the third story was larger than that of the uncontrolled specimen F.

To understand the response tendency of the proposed system, the distributions of the maximum acceleration response and displacement under the Art-wave with 40%, 60%, and 80% excitations are summarized in Figure 18, focusing on FWD(Z+Z) and FWD(Z-Z). The maximum displacement response of both specimens increased with increasing input levels while maintaining the deformation shape, whereas the acceleration response exhibited significant variability in shape depending on the input level. A conspicuous feature is that FWD(Z+Z) reduced the acceleration response in the third and sixth stories where the wires were installed; however, FWD(Z-Z) increased the response in the third and sixth stories.

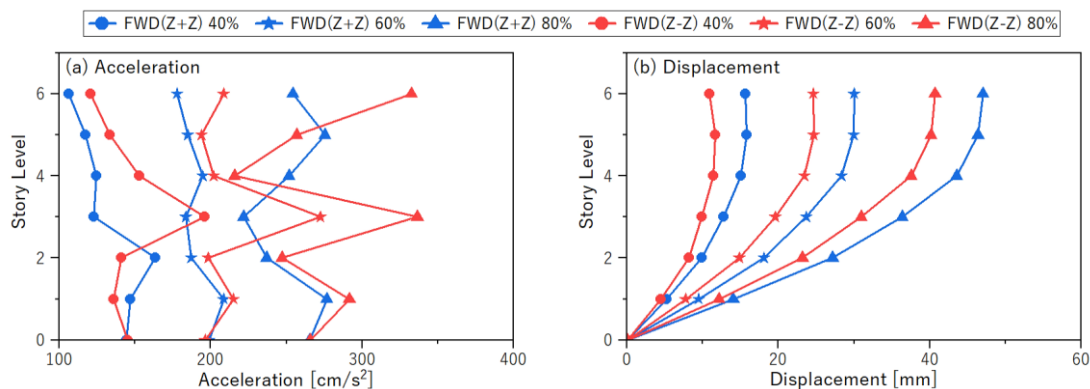


Figure 18. Transition of maximum displacement and acceleration response under Art-wave with 40 %, 60 %, and 80% excitations

To investigate the characteristics of the acceleration response in more detail, a wavelet-based analysis, which can provide information on the variable frequencies and intensities of the time-history data in the time domain, was applied to the recorded acceleration data in both FWD(Z+Z) and FWD(Z-Z). Figure 19 shows the acceleration time history on

the sixth story and its wavelet power spectrum under the Art-wave with 80% excitation ($PGA\ 265\ cm/s^2$). A significant difference between FWD(Z+Z) and FWD(Z-Z), as indicated by the wavelet-power spectrum, lies in the presence or absence of a response at approximately 5 Hz. In the case of FWD(Z-Z), the influence of the higher mode deformation was evident in the acceleration response, leading to a greater presence of small noise in the acceleration time history compared with FWD(Z+Z). This occurrence of second-mode vibration was attributed to the wire layout of the FWD(Z-Z) specimen, which was designed for first-mode deformation, thereby limiting the effectiveness of the response reduction under the second vibration mode. In contrast, the discontinuous wire layout of FWD(Z+Z) provided a response-mitigation effect regardless of the vibration modes.

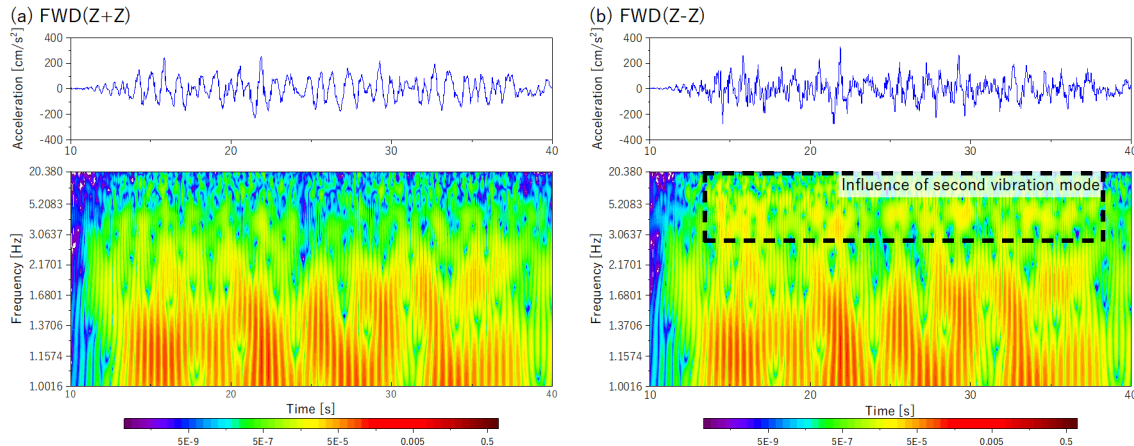


Figure 19. Acceleration time history and wavelet power spectrum on the sixth story

5.4. Displacement-Amplification Factor

The displacement-amplification effect of all wire layouts was verified. Figure 20 shows a comparison of the experimental and theoretical wire displacement time history in terms of the relative displacement. The relative displacement of the wire was obtained by subtracting the lower wire movement, and the theoretical wire displacement was calculated by multiplying the amplification factor by the relative displacement between the pulley-installed stories. In addition, the cumulative displacement of the wire and story was calculated, and the cumulative displacement-amplification ratio (displacement amplification factor) was obtained by dividing the cumulative displacement by the cumulative displacement of the story.

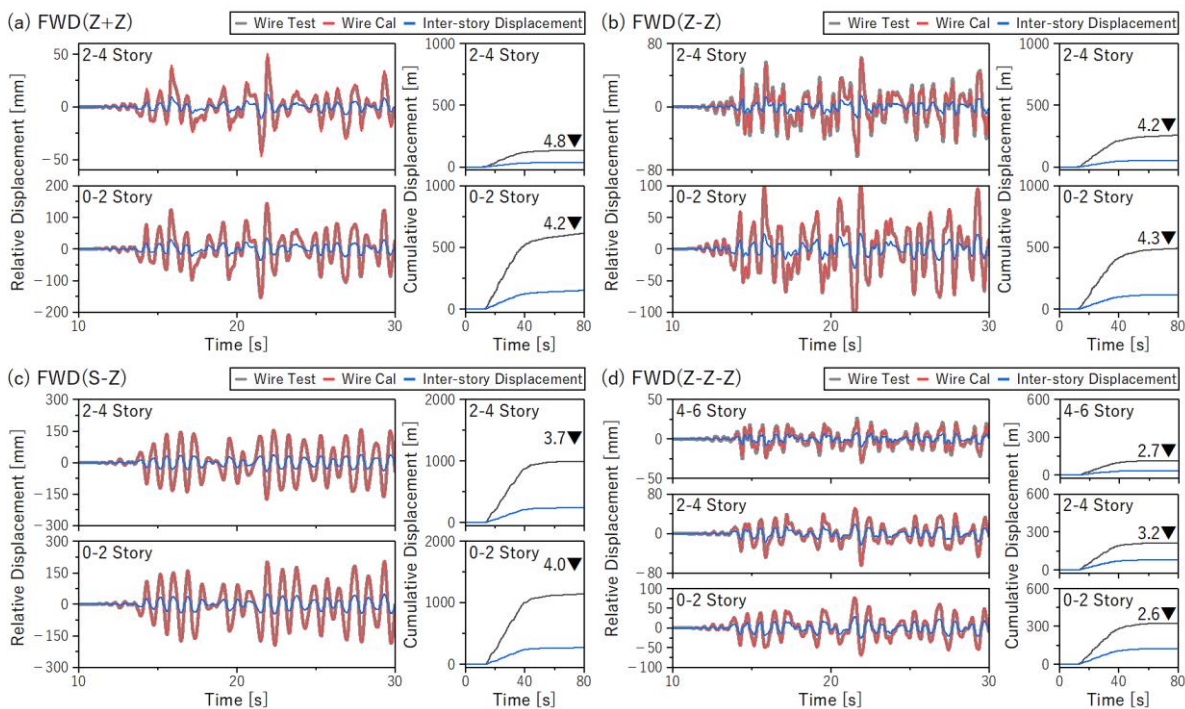


Figure 20. Comparison of the test and theoretical displacement of the wire and the cumulative displacement under Art-wave with 80 % excitation ($PGA\ 265\ cm/s^2$)

As shown in Figure 20, the wire displacement recorded during the test and the theoretically calculated wire displacement align closely across all specimens. As indicated by the displacement amplification factor in Figure 20, although some variation was observed, a displacement amplification factor close to the theoretical value (4.2 for (Z+Z), (S-Z), and (Z-Z), and 2.7 for (Z-Z-Z), respectively) was achieved. Additionally, the agreement between the maximum points of experimental measurements and theoretical values suggests that the wire maintained high rigidity during excitations and did not experience severe elongation. Furthermore, the consistency of the time-history waves demonstrates that the fundamental theoretical equation expressed in Equation 1, even without considering sheave friction and wire elongation, accurately predicts the actual wire displacement under different specimen configurations.

5.5. Energy Absorption

Figure 21 shows the hysteresis of the force-deformation relationship for the friction and rotational dampers and the time history of the cumulative energy absorption. The proposed systems were installed at both the front and back of the specimen; thus, the total energy absorbed by the damper system was estimated to be double that absorbed by the front system. Here, the input and decapitated energies of the proposed damper system were estimated using the following equations:

$$E = - \sum_0^N \int_0^t \dot{x}_i(t) m_i \ddot{z}_0(t) \Delta t \tag{6}$$

$$W_d = \int_0^t F_d(t) \dot{u}_w(t) \Delta t \tag{7}$$

where \dot{x}_i is the relative velocity of the i th story, m_i is the mass of the i th floor, \ddot{z}_0 is the absolute acceleration at the shaking-table surface, N is the number of stories, F_d is the damping force of the friction and rotational dampers, and \dot{u}_w is the velocity of the wire. Here, the damping force and friction force were calculated from the difference in wire tension obtained by the load cells similar with the element tests in section 4.2 and 4.3.

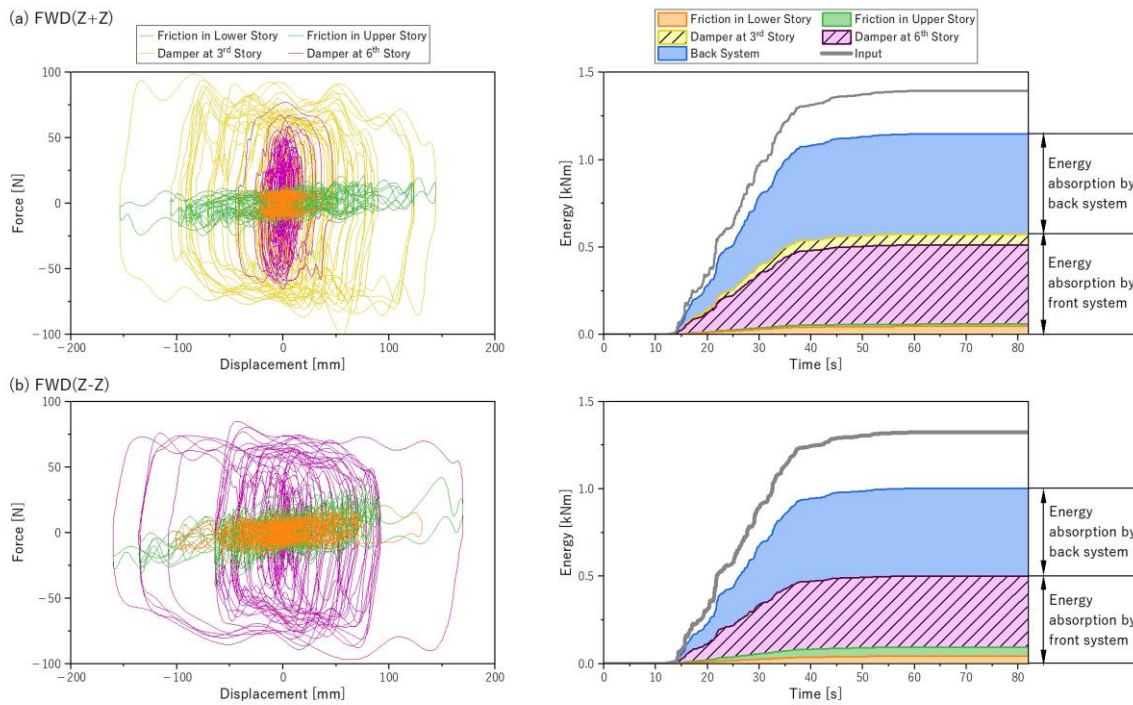


Figure 21. Hysteresis curves of friction and damper and the energy-dissipation time history

For FWD(Z+Z), the relative displacement in the lower story was larger than that in the upper story. Consequently, the energy absorption by the viscous damper placed on the sixth story was limited, with another viscous damper absorbing 33% of its input energy. In contrast, specimen FWD(Z-Z), which used a continuous wire and had only one viscous damper on the sixth story, absorbed 31% of the input energy. Therefore, the proposed system had the potential to utilize the energy-dissipation capacity of individual dampers efficiently and effectively by leveraging the cumulative amplified displacement across multiple stories.

Additionally, Figure 22 shows the distribution of the energy absorption for the input energy under Art-wave with 80 % (PGA 265 cm/s²) excitation. Except for specimen FWD(S-Z), which was inadequate for reducing seismic response, specimens FWD(Z-Z) and FWD(Z-Z-Z) with a continuous wire and single-damper system achieved an energy-absorption rate (ratio of input energy to energy absorbed by the damper system) of over 70 %. This performance was comparable to that of specimen FWD(Z+Z), which used a discontinuous wire and had two dampers located on the middle and top stories.

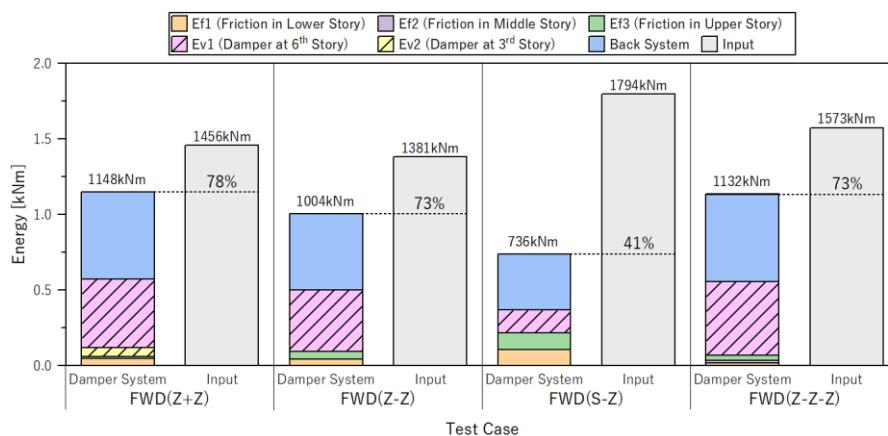


Figure 22. Distribution of the energy absorption and energy-absorption rate

6. Conclusions

This study presented an innovative passive vibration-control system, called the PDMAS, which incorporated pulley mechanisms to amplify the damper displacement and enhance energy dissipation in multi-story structures. The working principle of the proposed system was discussed, and an experimental investigation confirmed its potential as an effective passive vibration-control system for multi-story structures. The main conclusions of this study are as follows:

- The benefit of the PDMAS is that it improved the energy-absorption efficiency of individual dampers by utilizing the cumulative amplified story displacement through a continuously stretched cable across the entire structure. In addition, the proposed system had significant potential for controlling the responses induced by higher vibration modes by devising a wire-installation layout.
- A series of comparative shaking-table tests were conducted to confirm the feasibility of the PDMAS and the effectiveness of its seismic response reduction. Nine specimens were prepared with and without dampers under different wire-installation layouts. The operation of delivering the cumulative amplified story displacement to the damper was successfully verified without any issues, such as the tangling of the wire during excitations. Furthermore, the expected displacement-amplification factor of the pulley mechanism was obtained, and an accurate displacement-amplification effect was confirmed by comparing the axolemmal and theoretical results.
- The impact of various wire-installation layouts on seismic mitigation was examined. The PDMAS effectively reduced the overall story response, whereas previous experiments using PDAS in a coupled structure primarily mitigated the response at the connected story. Additionally, the continuous wire configuration significantly reduced the displacement response compared to the discontinuous wire configuration, though the acceleration response was slightly larger due to the influence of higher mode vibrations.
- The shaking table test results on the proposed system revealed that a specimen equipped with a single damper featuring a continuous wire layout from the bottom through the middle story to the top could provide a comparable energy-absorption rate and better displacement reduction than a specimen equipped with two dampers using a discontinuous wire layout in the lower and upper stories. This finding proved that accommodating the cumulative displacement effectively improved the energy-absorption capacity of the individual dampers and indicated the possibility of reducing the number of dampers.
- The major concern regarding the continuous wire layout along the building height is that it is ineffective for activating the damper capacity under the second-mode response because the cumulative inter-story displacements in the lower and upper structures are mutually cancelled. To overcome this problem, a specimen with a continuous wire layout specially optimized for the second-vibration mode, which changed the direction of the wire at the middle story, was also tested. The effects of the displacement amplification and damping-force performance when the system was excited by a sinusoidal wave at its second vibration frequency were confirmed. However, because first-mode deformation was dominant under the selected simulated earthquake wave, the response-reduction effect was limited.

The response-reduction effect of the proposed system was examined using only one earthquake motion and several wire layouts. The PDMAS offers potential applicability in flexibly optimizing wire layouts based on the vibration mode of the target structure. For structures with irregular story weight distribution along the vertical axis, such as racking systems in logistic warehouses, the influence of higher mode vibrations must be taken into account. Implementing the PDMAS could be an effective solution to transmit cumulative displacement to the connected damper. The comprehensive response-reduction effect under several earthquake motions, capturing both near-fault and far-field, and the optimized design of the proposed system, such as the different number of wire loops as well as the location of pulleys, will be further investigated in a subsequent study.

7. Declarations

7.1. Author Contributions

Conceptualization, R.M. and T.S.; methodology, R.M., Y.Y., and T.S.; validation, R.M.; formal analysis, R.M.; investigation, R.M.; data curation, R.M.; writing—original draft preparation, R.M.; writing—review and editing, R.M., Y.Y., and T.S.; visualization, R.M.; supervision, T.S.; project administration, R.M. and Y.Y.; funding acquisition, R.M. and T.S. All authors have read and agreed to the published version of the manuscript.

7.2. Data Availability Statement

The data presented in this study are available on request from the corresponding author.

7.3. Funding

This work was financially supported by the JSPS KAKENHI Grant Number JP23KJ1143 and a grant from the Cooperative Project for Innovation Research Program funded by Toyohashi University of Technology.

7.4. Acknowledgements

The authors also gratefully acknowledge the support provided by Mr. S. Sakai (Hazama Ando Corp.), Mr. M. Uchikawa (Sato Kogyo Co., Ltd.), Mr. E. Nishimura (Toda Corp.), Mr. H. Ryujin (Maeda Co., Ltd.), Mr. R. Doi (Kumagai Gumi Co., Ltd.), and T. Kanada (Cooperative Research Facility Center, Toyohashi University of Technology).

7.5. Conflicts of Interest

The authors declare no conflict of interest.

8. References

- [1] Kavyashree, B., Patil, S., & Rao, V. S. (2021). Review on vibration control in tall buildings: from the perspective of devices and applications. *International Journal of Dynamics and Control*, 9(3), 1316–1331. doi:10.1007/s40435-020-00728-6.
- [2] Symans, M. D., Charney, F. A., Whittaker, A. S., Constantinou, M. C., Kircher, C. A., Johnson, M. W., & McNamara, R. J. (2008). Energy Dissipation Systems for Seismic Applications: Current Practice and Recent Developments. *Journal of Structural Engineering*, 134(1), 3–21. doi:10.1061/(asce)0733-9445(2008)134:1(3).
- [3] Lagos, R., Kupfer, M., Lindenberg, J., Bonelli, P., Saragoni, R., Guendelman, T., Massone, L., Boroschek, R., & Yañez, F. (2012). Seismic performance of high-rise concrete buildings in Chile. *International Journal of High-Rise Buildings*, 1(3), 181-194.
- [4] Constantinou, M. C., Tsopeles, P., Hammel, W., & Sigaher, A. N. (2001). Toggle-Brace-Damper Seismic Energy Dissipation Systems. *Journal of Structural Engineering*, 127(2), 105–112. doi:10.1061/(asce)0733-9445(2001)127:2(105).
- [5] Şigaher, A. N., & Constantinou, M. C. (2003). Scissor-jack-damper energy dissipation system. *Earthquake Spectra*, 19(1), 133–158. doi:10.1193/1.1540999.
- [6] Kang, J. Do, & Tagawa, H. (2014). Experimental evaluation of dynamic characteristics of seesaw energy dissipation system for vibration control of structures. *Earthquake Engineering and Structural Dynamics*, 43(12), 1889–1895. doi:10.1002/eqe.2420.
- [7] Feng, H., Zhou, F., Ge, H., Zhu, H., & Zhou, L. (2021). Energy dissipation enhancement through multi-toggle brace damper systems for mitigating dynamic responses of structures. *Structures*, 33, 2487–2499. doi:10.1016/j.istruc.2021.05.068.
- [8] Alhasan, A. A., Vafaei, M., & C. Alih, S. (2025). Cyclic response and mechanical model of a rotational viscoelastic damper. *Engineering Structures*, 322. doi:10.1016/j.engstruct.2024.119117.
- [9] Lie, W., Zhou, Y., Zhang, Q., Hong, J., & Chen, Z. (2025). Potential use of rotational metallic dampers for seismic enhancement of infilled RC frames with open first story. *Engineering Structures*, 322. doi:10.1016/j.engstruct.2024.119080.
- [10] Wu, X., Ji, P., Liu, C., Li, L., Zhao, Z., & Zhang, Z. (2024). Experimental and numerical investigation of a novel passive energy dissipation system with viscoelastic damper and angle-reaction controller. *Soil Dynamics and Earthquake Engineering*, 187. doi:10.1016/j.soildyn.2024.108939.
- [11] Ma, R., Cheng, Z., Zhang, X., Bi, K., & Jiang, S. (2024). Mechanical behaviors and seismic performance of a novel rotary amplification friction damper (RAFD): Experimental and analytical studies. *Journal of Constructional Steel Research*, 223. doi:10.1016/j.jcsr.2024.109051.
- [12] Pekcan, G., Mander, J. B., & Chen, S. S. (2000). Experiments on Steel MRF Building with Supplemental Tendon System. *Journal of Structural Engineering*, 126(4), 437–444. doi:10.1061/(asce)0733-9445(2000)126:4(437).
- [13] Pekcan, G., Mander, J. B., & Chen, S. S. (2000). Balancing Lateral Loads Using Tendon-Based Supplemental Damping System. *Journal of Structural Engineering*, 126(8), 896–905. doi:10.1061/(asce)0733-9445(2000)126:8(896).

- [14] Sorace, S., & Terenzi, G. (2011). The damped cable system for seismic protection of frame structures — Part I: General concepts, testing and modeling. *Earthquake Engineering & Structural Dynamics*, 41(5), 915–928. doi:10.1002/eqe.1166.
- [15] Sorace, S., & Terenzi, G. (2012). The damped cable system for seismic protection of frame structures - Part II: Design and application. *Earthquake Engineering and Structural Dynamics*, 41(5), 929–947. doi:10.1002/eqe.1165.
- [16] Choi, H., & Kim, J. (2010). New installation scheme for viscoelastic dampers using cables. *Canadian Journal of Civil Engineering*, 37(9), 1201–1211. doi:10.1139/L10-068.
- [17] Kurata, M., Leon, R. T., & DesRoches, R. (2012). Rapid Seismic Rehabilitation Strategy: Concept and Testing of Cable Bracing with Couples Resisting Damper. *Journal of Structural Engineering*, 138(3), 354–362. doi:10.1061/(asce)st.1943-541x.0000401.
- [18] Mehrabi, M. H., Ibrahim, Z., Ghodsi, S. S., & Suhatri, M. (2019). Seismic characteristics of X-cable braced frames bundled with a pre-compressed spring. *Soil Dynamics and Earthquake Engineering*, 116, 732–746. doi:10.1016/j.soildyn.2018.10.014.
- [19] Hernández, F., Astroza, R., Beltrán, J. F., Zhang, X., & Mercado, V. (2022). A experimental study of a cable-pulleys spring-damper energy dissipation system for buildings. *Journal of Building Engineering*, 51, 104034. doi:10.1016/j.job.2022.104034.
- [20] Kang, J., Xue, S., Xie, L., Tang, H., & Zhang, R. (2023). Multi-modal seismic control design for multi-storey buildings using cross-layer installed cable-bracing inerter systems: Part 1 theoretical treatment. *Soil Dynamics and Earthquake Engineering*, 164. doi:10.1016/j.soildyn.2022.107639.
- [21] Saito, T., Maegawa, T., Denno, S., Sakai, S., Uchikawa, M., Kanagawa, M., & Ryujin, H. (2017). New seismic response control system using block and tackle. 16th World Conference on Earthquake Engineering, 9-13 January, 2017, Santiago, Chile.
- [22] Jung, I. Y., Ryu, J., Oh, J., Ryu, D., & Ko, H. J. (2021). Experimental investigation on displacement amplification mechanism of steel wire rope-pulley damping systems with viscous damper. *Engineering Structures*, 248, 113206. doi:10.1016/j.engstruct.2021.113206.
- [23] Rouhani, B., Aghayari, R., & Mousavi, S. A. (2024). Fluid viscous dampers in tackle-damper configuration: An experimental study. *Engineering Structures*, 321. doi:10.1016/j.engstruct.2024.118927.
- [24] Majima, R., Hayashi, K., & Saito, T. (2022). Development of new passive vibration control system in coupled structures with block and tackle. *Soil Dynamics and Earthquake Engineering*, 159, 107319. doi:10.1016/j.soildyn.2022.107319.
- [25] Chung, Y.-L., Nagae, T., Hitaka, T., & Nakashima, M. (2010). Seismic Resistance Capacity of High-Rise Buildings Subjected to Long-Period Ground Motions: E-Defense Shaking Table Test. *Journal of Structural Engineering*, 136(6), 637–644. doi:10.1061/(asce)st.1943-541x.0000161.
- [26] Kaneko, M., Kumagai, H., & Okada, K. (2016). Development of 3-Dimensional Large-Scale Shaking Table and 3-Dimensional Long-stroke Shaking Table. *Journal of Japan Association for Earthquake Engineering*, 16(9), 100-117. doi:10.5610/jaee.16.9_100.
- [27] Mukai, Y., & Fujitani, H. (2019). Development of Resilient Seismic Response Control with a Semi-active System: Seismic Isolation, Structural Health Monitoring, and Performance Based Seismic Design in Earthquake Engineering, Springer, Cham, Switzerland. doi:10.1007/978-3-319-93157-9_2.
- [28] Tani, T., Ishikawa, Y., Maseki, R., & Nakajima, T. (2023). Shaking Table Test of the High-Damping Structural System with Multi-Story Shear Walls and Dampers. *AIJ Journal of Technology and Design*, 29(71), 62–67. doi:10.3130/AIJT.29.62.
- [29] Katsimpini, P. S., Askouni, P. K., Papagiannopoulos, G. A., & Karabalis, D. L. (2020). Seismic drift response of seesaw-braced and buckling-restrained braced steel structures: A comparison study. *Soil Dynamics and Earthquake Engineering*, 129, 105925. doi:10.1016/j.soildyn.2019.105925.
- [30] Mousavi, S. A., & Zahrai, S. M. (2017). Slack free connections to improve seismic behavior of tension-only braces: An experimental and analytical study. *Engineering Structures*, 136, 54–67. doi:10.1016/j.engstruct.2017.01.009.